Earth and Planetary Science Letters 299 (2010) 368–381

Contents lists available at ScienceDirect

Earth and Planetary Science Letters

journal homepage: www.elsevier.com/locate/epsl

Mineralogical and chemical variability of fluvial sediments 1. Bedload sand (Ganga–Brahmaputra, Bangladesh)

Eduardo Garzanti [a,*], Sergio Andò [a,1], Christian France-Lanord [b,2], Giovanni Vezzoli [a,1], Paolo Censi [c,3], Valier Galy [b,4], Yani Najman [d,5]

[a] Laboratorio di Petrografia del Sedimentario, Dipartimento di Scienze Geologiche e Geotecnologie, Università di Milano-Bicocca, 20126 Milano, Italy
[b] Centre de Recherches Pétrographiques et Géochimiques, BP 20, 54501 Vandoeuvre-lès-Nancy, France
[c] Dipartimento CFTA, Università di Palermo, 90123 Palermo, Italy
[d] Department of Environmental Science, Lancaster University, LA1 4YQ Lancaster, UK

ARTICLE INFO

Article history:
Received 19 April 2010
Received in revised form 15 September 2010
Accepted 16 September 2010
Available online 15 October 2010

Editor: M.L. Delaney

Keywords:
sedimentary geochemistry
sedimentary petrology
settling equivalence
selective entrainment
placer sands
opaque minerals
REE-bearing minerals
Eu anomaly
Himalaya

ABSTRACT

This study investigates the natural processes that control concentration of detrital minerals and consequently chemical elements in river sand. The novelty of our approach consists in the systematic integration of detailed textural, petrographical, mineralogical and chemical data, and in the quantitative description and modeling of relationships among mineralogical and chemical variables for each sample and each grain-size class in each sample. Bed sediment in transit in the largest sedimentary system on Earth chiefly consists of fine-grained lithofeldspathoquartzose sand including rich amphibole–epidote–garnet suites, mixed with minor very-fine-grained-sand to silt subpopulations containing less heavy minerals and representing intermittent suspension. Mineralogical and particularly chemical differences between Ganga and Brahmaputra bedload are orders of magnitude less than both intersample variability associated with selective-entrainment effects and intrasample variability associated with settling-equivalence effects. Any provenance interpretation of mineralogical, chemical, or detrital-geochronology datasets therefore requires quantitative understanding of hydraulically controlled compositional variability. Mineralogical and chemical, intrasample and intersample variability can be deduced with simple equations and numerical solutions. The underlying assumptions on the chemical composition of detrital minerals, as well as the possible pitfalls, uncertainties and approximations involved are discussed. Principal results include calibration of rare REE-bearing ultradense minerals, ill-determined by optical analyses but crucial in both detrital-geochronology and settling-equivalence studies, and assessment of progressively changing concentration for any detrital component with increasing intensity of selective-entrainment effects. Contributions by each mineral group to the chemical budget were inferred with sufficient precision and accuracy. Although complex because of diverse controlling factors including provenance, weathering and anthropogenic pollution, mineralogical and consequently chemical variability of fluvial sediments can be quantitatively predicted. This path, difficult because of insufficient information but far from hopeless, shall eventually lead to more accurate calculation of sediment fluxes and chemical budgets, as well as to a deeper understanding of sedimentary geochemistry and fluvial sedimentology.

> *"The sands of the river Ganga are violently trampled on by fishes, tortoises, porpoises, crocodiles, buffaloes, lions, elephants, but the sands are not troubled, have no ill feelings, nor are they unconscious of being trampled on; they are without imagination, beautifully clear and devoid of impurities. The sands of the river Ganga flow along the stream and are permanent, and so is the essence of Buddahood."* Mahayana Lankavatara Sutra, The parable of the sands of the Ganga

1. Introduction

The physical characteristics of turbulent river-flows vary rapidly, irregularly, and by orders of magnitude in space and time. Moreover, data from a big river in flood, when the bulk of sediment transport

* Corresponding author. Tel.: +39 02 64482088; fax: +39 02 64482073.
E-mail addresses: eduardo.garzanti@unimib.it (E. Garzanti), sergio.ando@unimib.it (S. Andò), cfl@crpg.cnrs-nancy.fr (C. France-Lanord), giovanni.vezzoli@unimib.it (G. Vezzoli), censi@unipa.it (P. Censi), vgaly@whoi.edu (V. Galy), y.najman@lancaster.ac.uk (Y. Najman).
[1] Tel.: +39 02 64482097, +39 02 64482069; fax: +39 02 64482073.
[2] Tel.: +33 383 594220; fax: +33 383 511798.
[3] Also at IAMC-CNR UOS di Capo Granitola, 91026 Campobello di Mazara (Trapani), Italy. Tel.: +39 091 23861638; fax: +39 091 347990.
[4] Now at Woods Hole Oceanographic Institution, 360 Woods Hole Road, Woods Hole, MA 02543, USA.
[5] Tel.: +44 1524 593898; fax: +44 1524 593985.

0012-821X/$ – see front matter © 2010 Elsevier B.V. All rights reserved.
doi:10.1016/j.epsl.2010.09.017

takes place, are not easily obtained. Our knowledge of detrital fluxes, distribution of sediments through the water column, and hydraulic control on their composition is consequently modest at best. Bedload fluxes are generally unknown, and we often rely on unproven assumptions such as that they represent some 10% of suspended or total load (Hay, 1998).

Mineralogical and chemical composition of sediments offer us an opportunity to investigate hydrodynamic processes during transport and deposition, but our knowledge on how detrital minerals are segregated by size–density and size–shape sorting into distinct size classes by different transport modes is still limited (Komar, 2007). Because diverse chemical elements are preferentially contained in minerals with different density or shape (e.g., Rb, Cs in slow-settling platy mica, Zr, Hf in fast-settling dense zircon), hydrodynamic processes that control mineralogical variability control chemical variability as well (McLennan et al., 1993; Ohta, 2004). By quantifying size–density–shape relationships among detrital minerals entrained on the channel bed, we can assess hydrodynamic impact on mineralogical and thus chemical composition of bedload sand. But in order to do this we must know how various chemical elements are hosted in different detrital minerals. A deeper understanding of such aspects is needed to correctly calculate relative contributions from multiple sediment sources, and thus to make accurate estimates of detrital fluxes, sediment budgets, and erosion rates based on mineralogical or chemical composition of sediments.

The present article quantitatively analyses the physical processes that control concentration of detrital minerals and consequently chemical elements in bedload sand. It represents the first part of a detailed investigation on fluvial sediment in transit, the second part being dedicated to mud carried in suspension (Garzanti et al., in press). As a giant natural laboratory, we used the Ganga–Brahmaputra fluviodeltaic system in Bangladesh. This is the largest entry point of detritus in the world oceans, which has fed throughout the Neogene the huge turbidite fan expanding on Bengal Sea floors (France-Lanord et al., 1993; Goodbred and Kuehl, 2000). Our work is based on a continuing research project carried out by CNRS-CRPG researchers during the full monsoon season through the last decade (Galy and France-Lanord, 1999; Galy et al., 2007; Singh and France-Lanord, 2002). The novelty of our approach consists in the systematic integration of textural, petrographical, mineralogical and chemical databases, and in the quantitative description and modeling of relationships among mineralogical and chemical variables for each sample and each grain-size class in each sample.

Mineralogical and chemical scrutiny of an active fluviodeltaic system allows us to constrain how and to what extent sediment composition is modified physically and chemically during transfer from detrital sources to depositional sinks, a fundamental requisite to make accurate quantitative provenance diagnoses. Unraveling mineralogical fractionation in deltaic environments is specifically needed to compare the composition of fluvial and turbidite deposits, and thus to unambiguously trace detrital signatures from mountain belts to ocean floors (Ingersoll et al., 2003). The same knowledge is crucial for provenance analysis of ancient sandstone wedges, and may eventually enable us to unravel the full record of paleotectonic and paleoclimatic events stored in sedimentary archives. Practical applications of economic interest include a better understanding of detrital fluxes, soil erosion, lifetime of reservoirs, mechanisms of placer formation, and prospecting of sedimentary ore deposits.

2. The Ganga–Brahmaputra sedimentary system

The huge drainage basins of Rivers Ganga and Brahmaputra (1,060,000 km^2 and 630,000 km^2, respectively) include large tracts of the Himalayan belt as well as Precambrian basement of the Indian craton (Gansser, 1964). The two rivers join in central Bangladesh to form the Padma–Meghna estuary, strongly influenced by 4.5–6 m tides and delivering annually to the Bay of Bengal ~10^3 km^3 of water and $\geq 1.5\ 10^6$ t of sediment, most of which during the monsoon season (Fig. 1). Estimates of suspended load are $549 \pm 55\ 10^6$ t/yr for the Ganga and $\leq 1157\ 10^6$ t/yr for the Brahmaputra (Islam et al., 1999; RSP, 1996). Bedload is undetermined, and might even reach as high as the suspended load (Bristow, 1987).

During the rainy season, when water discharge peaks to 70,000–80,000 m^3/s, the Ganga becomes a large single meandering channel, reverting to a sandy braided course during the dry season (Singh, 2007). The Brahmaputra is an extremely dynamic, predominantly braided river with scours even 40–45 m deep (Coleman, 1969). In flood, water discharge may reach 100,000 m^3/s and the active braidplain 15–18 km in width. Sediment is mostly fine sand and silt, with <1% clay; bedload grain-size progressively decreases downstream. The dominant bedform are sand dunes, with heights ≤ 6 m, wavelengths ≤ 330 m, and migration rates ≤ 17 m/h. Although intense eddying may form slopes steeper than the angle of repose and up to 58°, average leeside angle is only 8°, suggesting absence of permanent large-scale flow separation. Smaller dunes and ripples are commonly superposed on larger dunes; upper-stage plane beds are largely restricted to fast, shallow flows on bar tops. Aeolian erosion and ripples to small barchanoid dunes may rework the top 10–50 cm of exposed bar surfaces. Even km-size composite bedforms including mid-channel and point bars are extremely mobile, whereas vegetated islands rising up to floodplain level are relatively stable ("chars"; Best et al., 2007).

3. Methods

Bedload in transit was sampled during the full monsoon season (July 2002, July 2004, July 2005, August 2007), from the channel bed at depths between 7.5 and 22 m, in Rivers Ganga (downstream of Hardinge Bridge), Brahmaputra (from Sirajganj to Jamuna Bridge), and Meghna estuary (near Bhola). In order to avoid contamination by suspended load, up to more than 1 kg of bedload sand was dredged with a stainless-steel tube equipped with a sampling bag, dropped to the bottom of the river and lifted after several minutes. Ganga, Brahmaputra and Padma fluvial bars were sampled during the dry pre-monsoon and post-monsoon seasons in April 2005, November 2005, and January 2008. Additional Ganga and Brahmaputra sands were collected upstream across the India–Bangladesh border from August 1996 to August 2001. Laser grain-size analyses were carried out at LEM-Nancy. The complete petrographic, mineralogical, and chemical database with information on sampling sites is provided in Appendix A.

3.1. Petrography and mineralogy

High-resolution bulk-petrography and heavy-mineral analyses were carried out for 21 samples. For 7 selected samples (bedload collected during the monsoon season and bar sands collected during the dry season for each of the three river branches, and Brahmaputra placer BR451) analyses were carried out separately for all significant size classes (multiple-window method; Garzanti et al., 2009). Samples were dry-sieved at 0.25 ϕ intervals, and each size class was impregnated with Araldite, prepared as standard thin sections, stained with alizarine red to distinguish calcite and dolomite, and point-counted by the Gazzi-Dickinson method (400 points; Ingersoll et al., 1984). This technique, removing effects related to breakage of coarse-grained rock fragments into their monomineralic constituents, is most appropriate to assess the component of size-dependent modal variability associated with depositional processes.

Following a simple nomenclature scheme (Dickinson, 1970), sands were classified according to their main components exceeding 10%QFL, (e.g., in a lithofeldspathoquartzose sand Q>F>L>10%QFL). From a quartered part of each size class, treated with sodium ditionite–

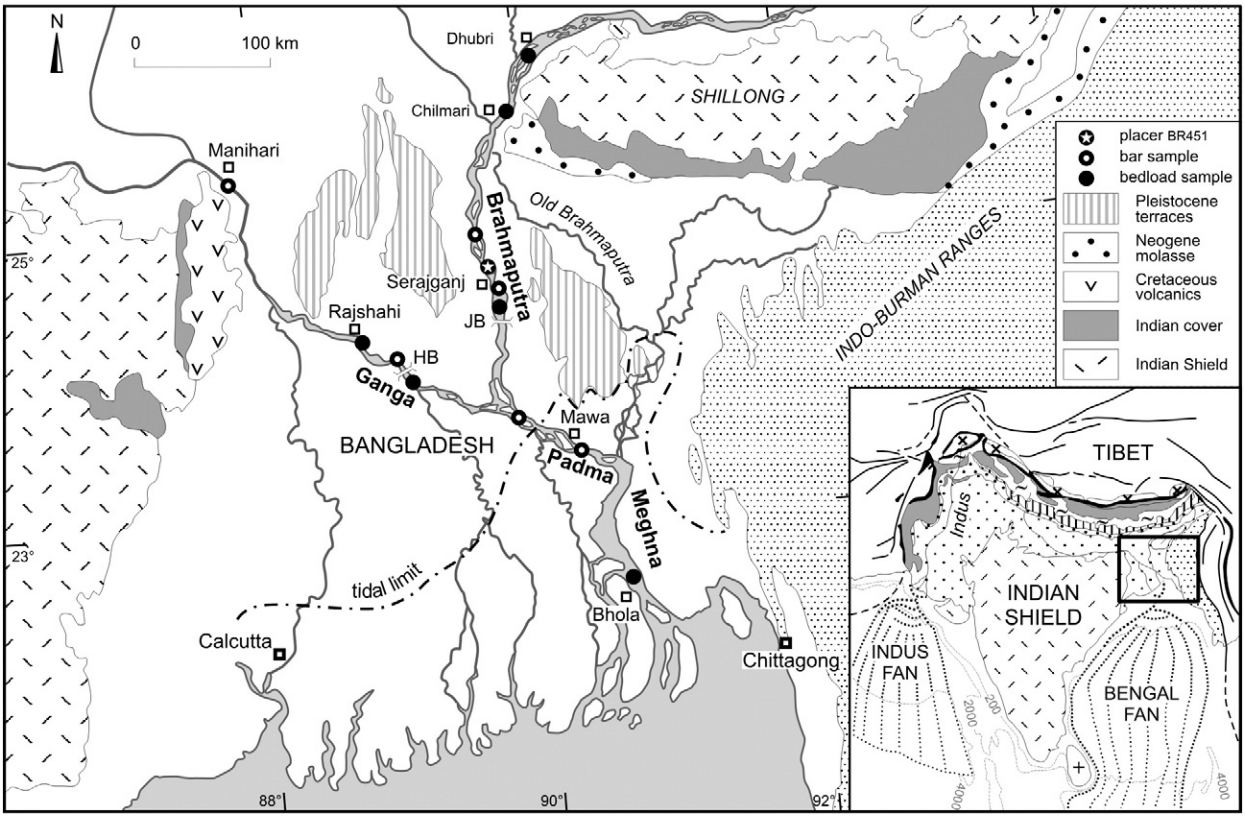

Fig. 1. The Ganga–Brahmaputra fluviodeltaic system in Bangladesh. Main geological features and location of studied bedload and bar samples are indicated. HB = Hardinge Bridge; JB = Jamuna Bridge.

citrate–bicarbonate to remove iron-oxide coatings, heavy minerals were separated by centrifuging in sodium metatungstate (density 2.90 g/cm^3), and recovered by partial freezing with liquid nitrogen. On grain mounts, 200 to 250 transparent heavy minerals were counted by the area-counting method (Mange and Maurer, 1992). Monazite and xenotime were determined by their distinctive absorption spectra revealed by a pocket spectroscope applied to the petrographic microscope (Hering and Zimmerle, 1963). Weathering features and percentages of unaltered, superficially corroded, deeply etched, and skeletal grains were determined for all counted heavy minerals in all classes. For each class, bulk-petrography modes were integrated with heavy-mineral modes by averaging the volume percentage of total heavy minerals, determined by point-counting in thin section, with the weight percentage of the heavy fraction separated in dense liquids, converted into volume percentage and depurated from spurious grains. For each sample, bulk-sediment composition was recalculated as the weighted average of integrated modes of each class. For each sample and class, heavy-mineral concentration was calculated as the volume percentage of total (HMC) and transparent (tHMC) heavy minerals. Heavy-mineral assemblages are described as "poor" (HMC<1), "moderately poor" (1≤HMC<2), "moderately rich" (2≤HMC<5), "rich" (5≤HMC<10) "very-rich" (10≤HMC<20), and "extremely rich" (20≤HMC<50).

3.2. Chemistry

Major and trace element concentrations in most bulk sand samples, heavy-mineral-rich finer classes, and mica-rich coarser classes were measured at CRPG-Nancy by ICP-AES and ICP-MS after alkaline fusion with lithium metaborate followed by acid digestion. The typical analytical precision of major element concentration is better than 2% (for full information on analytical procedures, geostandards used and precision for various elements see Carignan et al., 2001; Govindaraju and Mevelle, 1987; http://helium.crpg.cnrs-nancy.fr/SARM/index.html). Main grain-size subclasses, split by sieving at 0.50 ϕ (bar samples) or 0.25 ϕ intervals (placer BR451) were analysed at ACME Laboratories Vancouver (for detailed information on adopted procedures for group 4A–4B see http://acmelab.com/).

Composition of analysed sediments is discussed with reference to estimated average concentration of chemical elements in the upper continental crust (UCC; Hu and Gao, 2008; McLennan, 2001; Taylor and McLennan, 1995). REE data were normalized to CI carbonaceous chondrites (McDonough and Sun, 1995). Weathering indices were calculated using molecular proportions and correcting for CaO in apatite and carbonates; calcite and dolomite were manometrically determined as CO_2 released by selective reaction with >100% H_3PO_4 (Galy et al., 1999). Increasing alteration is indicated by increasing CIA (Chemical Index of Alteration; Nesbitt and Young, 1982) and PIA (Plagioclase Index of Alteration; Fedo et al., 1995), and by decreasing WIP (Weathering Index; Parker, 1970; Price and Velbel, 2003).

3.3. Combining mineralogical and chemical modes

The systematic use of combined mineralogical and chemical datasets represents a potentially formidable tool to investigate compositional variability of sediments. However, conversion of mineralogical into chemical composition is far from straightforward, and the opposite path virtually hopeless. For more than a century, normative mineralogy of igneous rocks – not necessarily bearing close resemblance to modal mineralogy – has been determined by distributing elements among a fixed set of proxy-minerals according to sets of pre-defined rules. Several attempts have been made to develop similar procedures for terrigenous sediments (Cohen and Ward, 1991; Cox and Lowe, 1996; Paktunc, 2001; Rosen et al., 2004). But unlike igneous or metamorphic parageneses, detrital assemblages

do not need to respect phase rules, and thus include numerous components, each potentially embracing the whole compositional spectrum displayed in diverse source rocks. Each chemical element is contributed in unknown proportions by different species, most of them solid solutions and containing impurities or inclusions. Moreover, during the sedimentary cycle chemical composition is affected to an undetermined extent by weathering and anthropogenic pollution. Mathematical solutions are thus virtually unlimited (Slaughter, 1989).

In this study, we converted mineralogical modes (weight percentages) into chemical modes to compare recalculated with real chemical composition, and used chemical data to infer mineralogy only in the specific case of rare REE-bearing minerals. In order to assess chemistry of detrital minerals, we recurred both to direct analyses of mineral separates and to a comprehensive set of mineral analyses compiled from the literature, giving specific attention to Himalayan studies. Full information on assumed mineral compositions and data sources is provided in Appendix B.

3.4. Raman spectroscopy

Raman spectroscopy was extensively used to achieve several goals. We determined altered or dubious minerals in order to check and improve accuracy of bulk-petrography and heavy-mineral data. We identified distinct species within mineral groups (e.g., albite versus Ca-plagioclase) in order to assign the correct chemical composition to major detrital components. We determined opaque and high-birefringence ultradense minerals, crucial to obtain a good fit for key chemical elements and to assess hydraulic-sorting effects. We Raman-counted (100 grains each) three thin sections of Ganga, Brahmaputra, and Padma sands, in order to obtain mineralogical modes (Bangs Rooney and Basu, 1994) to be compared with petrographic modes including rock fragments. In placer BR451, we Raman-counted (100 grains each) the opaque ultradense fraction of seven classes representing 94% of bulk sample (63 to 212 μm), mounted on standard SEM pin stubs to avoid the noise produced by the bonding resin and enhance the signal of Fe–Ti–Cr oxides. Six

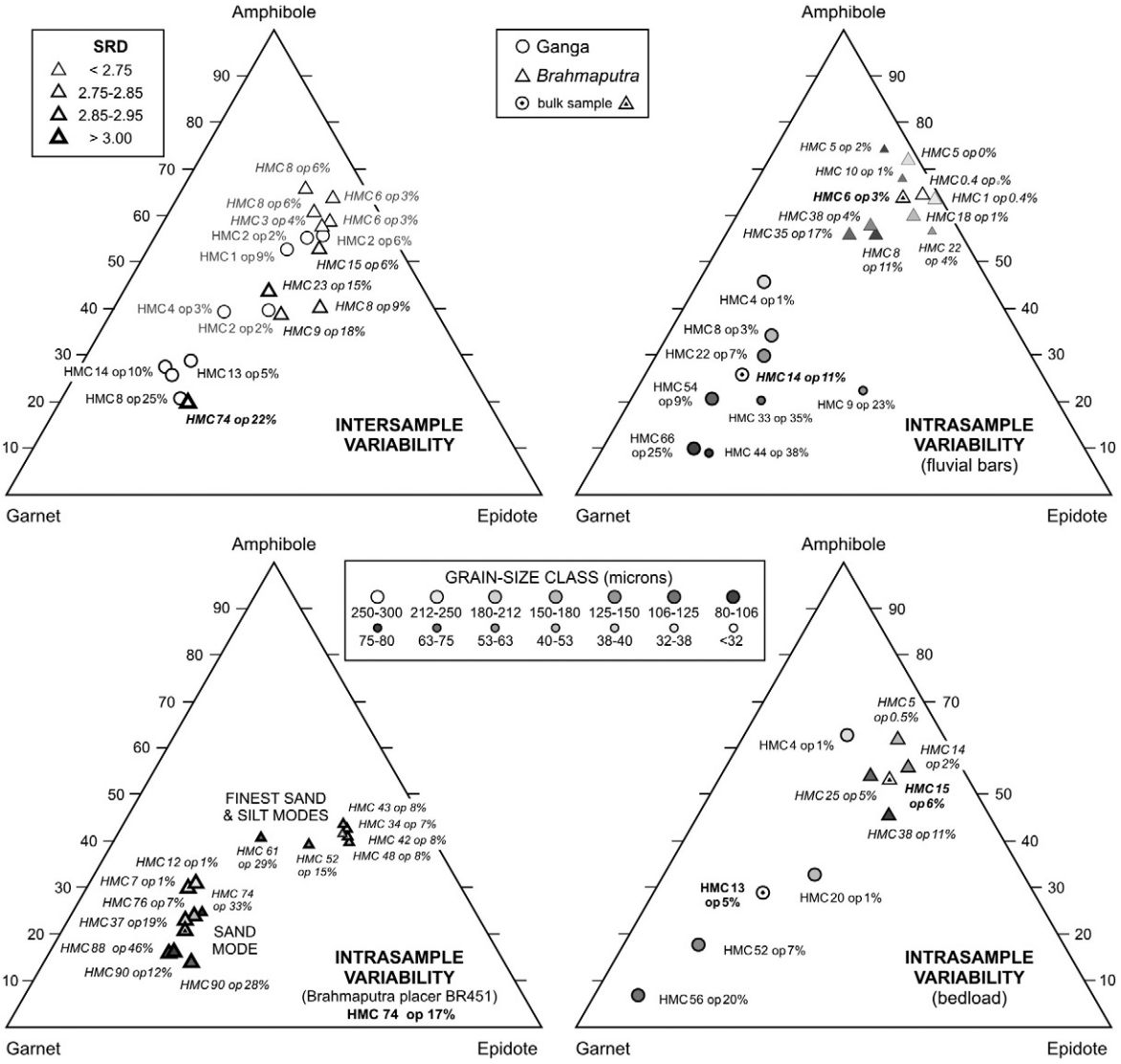

Fig. 2. Intersample and intrasample mineralogical variability. The three dominant mineral groups in collision-orogen detritus have different densities (amphibole ~ 3.2 g/cm^3; epidote ~ 3.45 g/cm^3; garnet ~ 4.0 g/cm^3). Their relative abundance, in different samples and different size classes of each sample, is consequently controlled by hydraulic effects, which dim provenance-related differences (e.g., higher garnet in Ganga sediments). Denser minerals (HMC = Heavy Mineral Concentration; op% = percentage of ultradense opaques on bulk sample) are enriched to different degrees in different samples because of selective-entrainment effects (upper left triangle), and systematically in finer classes of each sample because of settling-equivalence effects (upper right and lower right triangles). The settling-equivalence principle applies to both main sand mode and finer modes (lower left triangle).

classes of the coarse tail in bulk (300 to 1000 μm), for which only ~0.2 g were available overall, were also grain counted. Raman spectra were obtained on 1470 grains overall. For details on operational conditions and identification of diagnostic peaks see Garzanti et al. (in press).

4. Ganga–Brahmaputra bedload

4.1. Textures

All studied samples are fine-grained, well sorted, positively skewed, and leptokurtic. Brahmaputra sands ($2.1 \pm 0.4\,\phi$) tend to be coarser than Ganga ($2.3 \pm 0.3\,\phi$) and Padma–Meghna sands ($2.5 \pm 1.5\,\phi$). In more positively skewed and leptokurtic bar samples, the <32 μm class represents $0.14 \pm 0.02\%$ of total weight, suggesting possible post-depositional infiltration of cohesive mud (Matlack et al., 1989). For dredged bedload in transit, contamination by suspended load is prevented by the adopted sampling procedure, and occurrence of a long fine tail has to be considered primary (Friedman, 1967).

Size distribution of river sediments has long been envisaged as polymodal, resulting from mixing of approximately lognormally distributed subpopulations (Spencer, 1963; Tanner, 1964). Skewness and kurtosis of bulk distributions consequently reflect the relative magnitude and separation of distinct subpopulations (Ashley, 1978; Sun et al., 2002). Ganga–Brahmaputra bedload chiefly consists ($97 \pm 1\%$) of a well-sorted, nearly symmetrical and slightly leptokurtic upper-fine-sand mode ($2.3 \pm 0.2\ \phi$, $0.35 \pm 0.05\ \sigma_\phi$) moved by traction, with a subordinate ($3 \pm 1\%$) moderately-well-sorted, nearly symmetrical and mesokurtic lower-very-fine sand mode ($3.6 \pm 0.3\ \phi$, $0.45 \pm 0.15\ \sigma_\phi$) representing intermittent suspension (Middleton, 1976). Calculated settling velocities are 2.0–2.5 cm/s for the main sand mode and ~0.45 cm/s for the finest-sand mode. The same two modes, slightly finer-grained but with markedly higher grain density and thus similar settling velocities, characterize placer BR451, also including a third, very minor medium/coarse silt mode. The long fine tail of the size distribution may also include very small amounts of even finer modes, which for their very low settling velocity are almost homogeneously distributed through the water column (Vanoni, 2006).

4.2. Bulk-petrography and heavy minerals

Feldspatholithoquartzose to lithofeldspathoquartzose Ganga sands include metamorphic, limestone and dolostone lithic grains. Plagioclase (~60% albite, ~40% Ca-plagioclase) prevails over K-spar, and biotite over muscovite. Moderately-rich to very-rich garnet–amphibole–epidote suites include opaques, tourmaline, diopsidic clinopyroxene, kyanite, titanite, apatite, sillimanite, rutile, zircon, staurolite, monazite, chloritoid, and allanite. Lithofeldspathoquartzose Brahmaputra sands are richer in feldspar, lack carbonate grains, and include minor volcanic, metavolcanic, metabasite, and ultramafic lithic grains. Plagioclase (~40% albite, ~60% Ca-plagioclase) prevails over K-spar, and biotite over muscovite. Rich to very-rich amphibole–epidote–garnet suites include opaques, clinopyroxene, titanite, sillimanite, rutile, apatite, hypersthene, tourmaline, zircon, kyanite, staurolite, chloritoid, allanite, monazite, and rare Cr-spinel, enstatite, olivine, and xenotime.

Detrital garnets in the Ganga–Brahmaputra are pyralspites with dominant almandine and subordinate spessartine, pyrope, grossular, or andradite components (Andò et al. 2009); garnet grains with dominant spessartine or even andradite components were occasionally identified. In placer BR451, ultradense opaque grains are 44% ilmenite, 31% magnetite, 23% hematite, and 2% Cr-spinel. Among the over 12,000 counted unstable detrital minerals, only 6% pyroxene, 37% epidote 42% amphibole, and 79% garnet grains are unweathered; 41% pyroxene, 2% amphibole, a few epidote, garnet, and even opaque or staurolite grains are etched or exceptionally skeletal, reflecting weathering in monsoonal climate. All other minerals, including titanite, monazite, tourmaline and even zircon may be corroded. Marked differences of weathering features either between Ganga and Brahmaputra sands or among different size classes were not detected.

A third of studied samples have SRD ≥ 2.8, reflecting marked heavy-mineral concentration. The HMC index, never exceeding 8 in suspended load (Garzanti et al., in press), is >10 in many bedload samples and reaches as high as 74 in placer BR451 (SRD ~ 3.65), where all ultradense minerals (magnetite, ilmenite, zircon, monazite, xenotime, rutile, garnet, allanite, staurolite) are enriched by an order of magnitude or more relative to other samples. Less dense kyanite, chloritoid, titanite, epidote, pyroxene, amphibole, prismatic sillimanite, apatite, and tourmaline are less enriched, whereas the only heavy mineral depleted in placer BR451 is fibrolite. Enrichment trends are not significantly different in Ganga and Brahmaputra bedload, considering that Ganga bedload contains less heavy minerals than Brahmaputra bedload (HMC 5 ± 2 versus 8 ± 2, neglecting samples with anomalous SRD). This mainly because Ganga sand is richer in garnet derived from medium-grade Greater Himalaya metasediments, and consequently has a higher average heavy-mineral density than Brahmaputra sand, richer in hornblende and epidote largely derived from igneous and metaigneous rocks.

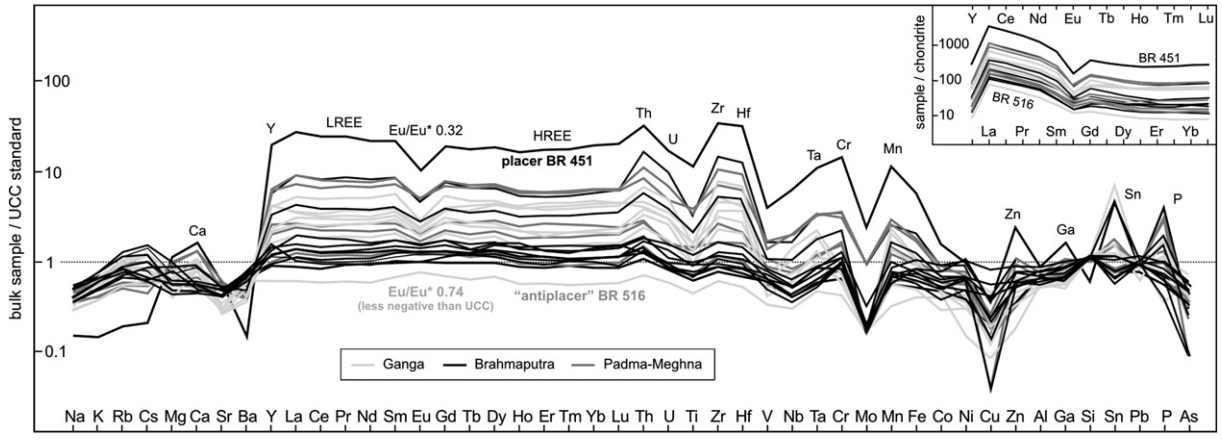

Fig. 3. Intersample chemical variability (elements in UCC-normalized multielement diagram arranged following the periodic table group by group). Inset shows chondrite-normalized YREE patterns. The nearly two-orders-of-magnitude variability in Y, REE, Th, U, Ti, Zr, Hf. Ta, Cr, and Mn (to a lesser extent in Ca, Zn, Ga, Sn, P), with extreme concentration in Brahmaputra placer BR451 and depletion in Ganga "antiplacer" BR516, is a selective-entrainment effect. Depletion in alkali and alkaline-earth metals (Na, Sr, Ba) and Mo is largely a weathering effect. Depletion in Co, Ni, Cu, Zn, Al, Ga, and As in most samples is a suspension-sorting effect (Garzanti et al., in press). Note strict hydraulic control on the Eu anomaly, most strongly negative in placer lags.

Because relative abundances of detrital minerals with contrasting densities are controlled by hydrodynamic processes (Fig. 2), the use of heavy-mineral ratios for provenance diagnosis may be misleading, unless hydraulic effects are assessed and removed. For instance, Huizing (1971) and Heroy et al. (2003) observed that epidote is more abundant than garnet in Brahmaputra sand and less abundant than garnet in Ganga sand; 30% of our samples, however, would be wrongly assigned according to such criterion.

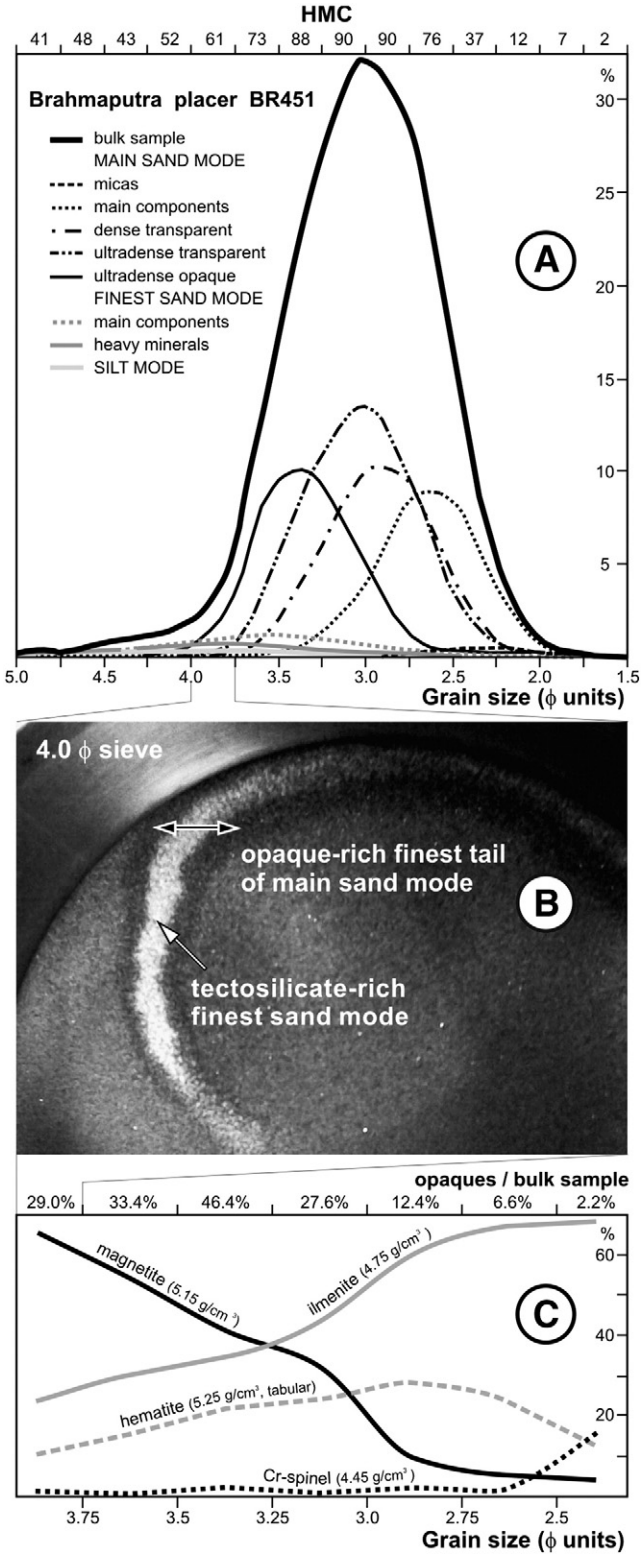

4.3. Geochemistry

Provenance-related differences in chemical composition are dimmed by overwhelming hydrodynamic effects (Fig. 3). Brahmaputra bedload tends to be richer in Na, Sr, Cr, Co, and Ni, reflecting more abundant plagioclase, amphibole and Cr-spinel, whereas Ganga bedload is richer in Ca, reflecting significant carbonate. In some samples, Y, REE, Th, U, Zr, Hf, and Cd are enriched by an order of magnitude relative to UCC, reflecting marked hydraulic concentration of ultradense minerals. Concentrations become extreme in placer BR451, where Th, Zr, Hf, and Cd are enriched 30–40 times relative to UCC, LREE 20–25 times (La most, Sm least), Y, HREE (Lu most, Ho least), U and Cr 15–20 times, Ti, Mn, Eu, and Ta 10–13 times, Nb and W 7–10 times, Fe, P, Sc, V, Ge, and Sn 4–6 times, and Mo, Zn, and Bi ~2 times. The degree of enrichment reflects the proportion in which each element is contributed by ultradense minerals (e.g., Zr, chiefly hosted in ultradense zircon, is more enriched than REE, hosted in monazite and xenotime but also in less dense garnet, allanite, titanite, epidote, apatite, amphibole). Depleted (Si, Al, Be, Sr, Pb) to strongly depleted (Na, K, Rb, Cs, Ba, Cu, As) in placer BR451 are elements mostly associated with tectosilicates and phyllosilicates, whereas elements associated also with heavy minerals are slightly enriched (Mg, Ca, Co, Ga).

Chondrite-normalized REE patterns display classical LREE enrichment, negative EU anomaly, and flat HREE distribution (Fig. 3; McLennan, 1989). The marked decrease from La to Sm (La_N/Sm_N 4.0 ± 0.3) reflects dominant monazite and allanite contribution. The lesser decrease from Gd to Ho (Gd_N/Ho_N 1.6 ± 0.2) reflects significant contribution also from titanite, having flatter REE patterns (Bea, 1996). The flat HREE pattern (Ho_N/Yb_N 1.0 ± 0.1) reflects contribution from xenotime, titanite, garnet, and subordinately zircon that has steep rising HREE pattern (Rubatto, 2002). REE contributions from diverse minerals are discussed in greater detail below, in Appendix B, and in Garzanti et al. (in press).

Hydraulic sorting may determine strong REE enrichment, but REE patterns vary slightly in our samples (La_N/Sm_N 4.0 ± 0.4, Gd_N/Ho_N 1.6 ± 0.2, Ho_N/Yb_N 1.0 ± 0.1). Only the Eu anomaly varies systematically, from Eu/Eu* 0.74 in REE-poor BR516 to 0.32 in placer BR451. Such trend reflects selective entrainment of low-density feldspar, typically displaying strongly positive Eu anomaly, and progressive concentration in placer lags of ultradense allanite and monazite, typically displaying strongly negative Eu anomalies (Bea, 1996). Provenance inferences based on the Eu anomaly, widely held as a conservative provenance proxy (Condie, 1993; Cullers, 1995; McLennan, 1989; Mongelli et al., 2006), may thus be misleading unless hydraulic bias is properly understood and removed.

Weathering indices are similar in Ganga–Brahmaputra bedload (CIA 55 ± 5) and Himalayan source rocks (CIA 50–65; France-Lanord and Derry, 1997; Singh et al., 2005; 2008), suggesting relatively limited silicate weathering (CIA_{UCC} 47; Singh, 2007, 2009). Plagioclase is largely preserved (PIA 55 ± 4 in Brahmaputra sand), but alkali and alkaline-earth metals are systematically depleted relative to UCC in all Ganga–Brahmaputra sediments (Fig. 3). Calcite is partly preserved in

Fig. 4. Polymodal size distribution of Brahmaputra placer BR451. A) The bulk-sample curve is a multimodal envelope that can be decomposed into a main sand and minor finest-sand and silt modes with different settling velocities. Each mode can be in turn decomposed in an ideally lognormal curve for each detrital species. The main sand mode is here subdivided into five mineralogical submodes: ultradense opaques (~5 g/cm^3); ultradense transparent minerals ($\geq$4 g/cm^3); other heavy minerals ($2.9 < \delta \leq 4$ g/cm^3); main framework components (quartz, feldspar, lithic fragments); slow-settling micas. Two submodes (heavy minerals; main framework components including micas) are shown for the finest-sand mode. The silt mode is undivided. B) Photo of 4.0 ϕ sieve shows that in the 4.0–3.75 ϕ class the dark-colored finest tail of the main sand mode chiefly consisting of ultradense opaques is mixed with the light-colored tectosilicate-rich central part of the finest-sand mode. C) Size–density–shape sorting of the ultradense opaque submode. Denser magnetite is concentrated in finer classes than less dense ilmenite and Cr-spinel; hematite should have the highest density, but it is roughly constant possibly due to its tabular shape.

Ganga sand but completely dissolved in Brahmaputra sand, as reflected by greater Ca depletion in the latter (Garzanti et al., 2005; Singh and France-Lanord, 2002).

Calculation of the WIP is strongly affected by both settling-equivalence and selective-entrainment effects. The WIP is particularly low in bedload (WIP 41 ± 7 vs. WIP_{UCC} 81) because slow-settling K-rich phyllosilicates are concentrated in suspended load, and even lower in placer BR451 (WIP 32, and as low as 17 in the fine tail), because slight enrichment in Mg and Ca only partially compensates for strong depletion in Na and K. Selective-entrainment effects cause minor discrepancies in the calculation of the CIA.

5. Settling equivalence and intrasample compositional variability

As selective entrainment is the primary cause of mineralogical and consequently chemical differences among bedload samples (intersample variability), settling equivalence is the primary cause of mineralogical and consequently chemical differences among grain-size classes of each sample (intrasample variability; Garzanti et al., 2009). These hydrodynamic processes can be modeled, and mineralogical and chemical composition of each sample and size class thus predicted.

5.1. Intrasample mineralogical variability

Because of settling-equivalence relationships among detrital minerals, denser grains concentrate systematically in the fine tail of sorted sediments, whereas the coarse tail is enriched in platy micas (Rittenhouse, 1943; Rubey, 1933). This process of size–density–shape sorting visibly operates even on subtle density differences within single mineral groups (Schuiling et al., 1985). Denser almandine or spessartine garnets are thus concentrated in finer classes with respect to less dense garnets with higher grossular or pyrope component (Andò et al., 2009). Among ultradense opaques in placer BR451, magnetite reaches maximum in finest sand, whereas less dense ilmenite and Cr-spinel progressively increase in very fine to fine sand (Fig. 4C).

Mixing with subordinate finest-sand to silt modes, to which the settling-equivalence principle also applies, is indicated by the occurrence of secondary peaks of quartz, feldspar and mica in finest sand and silt classes, as readily observed in the laboratory during sieving (Fig. 4B). Heavy-mineral concentration commonly shows a major peak at ~3 ϕ (fine tail of the main sand mode) and a minor peak in very coarse silt (fine tail of the finest-sand mode). The heavy-mineral suite of the main sand mode is richer in ultradense garnet, whereas the poorer suite of finer modes is relatively rich in less dense epidote (Fig. 2), as well as in amphibole, pyroxene, titanite, apatite, tourmaline, anatase/brookite. Different mineralogy of main sand and finer modes may result from hydraulic effects superposed on provenance effects (e.g., coarse garnet derived from Greater Himalayan amphibolite-facies metapelites versus fine aggregates of granular epidote and Ti-oxides derived from lower-grade Lesser Himalayan rocks). Because in fine sand ultradense minerals are 0.5–0.7 ϕ finer than quartz (Garzanti et al., 2008), less than the distance between the main sand and finest-sand modes, size curves invariably show a minimum at ~3.5 ϕ, a class containing the ultradense-mineral-rich finest tail of the main sand mode mixed with the coarse tail of the minor finest-sand mode (Fig. 4A).

5.2. Intrasample chemical variability

Because of settling-equivalence effects, chemical elements chiefly hosted in ultradense minerals are strongly concentrated in the fine tail of the size distribution (Fig. 5). Intrasample variability is much greater than intersample variability, finest classes being between two and three orders of magnitude richer in Zr than coarsest classes. In the fine tail of Ganga (S3559) and Brahmaputra (BR451) heavy-mineral-rich bedload, Zr and Cd are enriched 200–250 times relative to UCC, Hf 150–200 times, Th ~120 times, U ~90 times, LREE 70–75 times in S3559 and 50–60 times in BR451 (La most, Nd least), YHREE 40–70 times in S3559 and 30–50 times in BR451 (Gd most, Ho least), W up to 50 times in BR451, Sn up to 40 times in S3559, Cr up to 30 times in BR451, Eu and Ta 20–30 times, Ti 15–20 times, Nb and Bi 10–15 times, Fe, Mn and V 5–10 times, P, Sc, Zn, and Ge ~5 times, Mo, Co, Ni, Ga, Pb, and Sb ~2 times. Ca, Be, and Cu are similar to UCC, whereas Si, Al, Mg, Sr, and As are depleted, and Na, K, Rb, Cs, and Ba strongly depleted. Elements hosted in tectosilicates (Si, Na, Ca, Sr) reach their maximum abundance in the middle of the size distribution. Most elements, hosted in micas or associated impurities and inclusions (Al, Fe, Mg, K, Rb, Cs, Be, Ba, Y, REE, Th, U, Zr, Hf, V, Nb, Ta, Cr, Mo, W, Co, Ni, Cu, Zn, Cd, Ga, Sn, Pb, As, Sb, Bi), increase again in the coarsest tail. Ratios between elements also show regular trends. For instance, Zr/REE, Zr/P, Zr/Th and Zr/Y decrease systematically from as high as 6, 13, 35, and

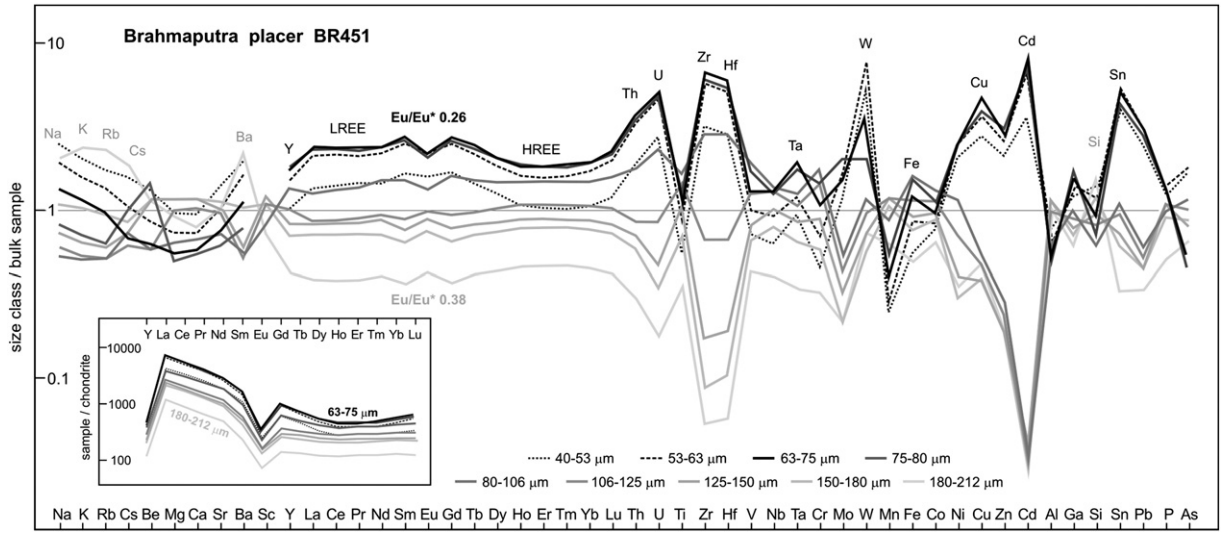

Fig. 5. Intrasample chemical variability in Brahmaputra placer BR451 (elements in multielement diagram normalized to bulk-sample composition and arranged following the periodic table group by group). Inset shows chondrite-normalized YREE patterns. Because of the settling-equivalence effect, Na, K, Rb, Cs, Ba, and Si are concentrated in the tectosilicate-rich upper-fine-sand class, and Y, REE, Th, U, Ti, Zr, Hf, V, Nb, Ta, Cr, W, Fe, Ni, Cu, Zn, Cd, and Sn in heavy-mineral-rich very-fine sand classes (but less so in very-coarse silt classes largely including finer modes poorer in heavy minerals). Note hydraulic control on the Eu anomaly, most strongly negative in the finest sand class.

64 in the fine tail of placer BR451, to respectively 0.4, 0.4, 4.7, and 3.5 in the modal class.

Differences in REE patterns among size classes of placer BR451 (e.g., La_N/Sm_N 5.6 ± 0.1, Gd_N/Ho_N 1.3 ± 0.1, Ho_N/Yb_N 0.91 ± 0.01, Eu/Eu* 0.38 ± 0.00 for fine-sand classes vs. La_N/Sm_N 4.3 ± 0.1, Gd_N/Ho_N 2.2 ± 0.1, Ho_N/Yb_N 0.85 ± 0.02, Eu/Eu* 0.28 ± 0.02 for coarsest-silt to finest-sand classes) reflect changing proportions of REE-bearing minerals, and indicate steeper LREE patterns for allanite than for denser monazite.

Settling-equivalence effects cause some discrepancies in the calculation of CIA (≤20% for all classes but the coarsest tail, where CIA increases by ~40%). This is largely because in the coarsest tail, where the increase in K is counterbalanced by the decrease in Na and Ca, Al increases more markedly than in the fine tail, where the moderate increase in Ca is counterbalanced by the decrease in Na and K. WIP markedly increases in the coarsest tail because both K and Mg increase.

5.3. Modeling intrasample mineralogical variability

The expected difference in nominal diameter between a detrital mineral with given density and shape relative to settling-equivalent quartz, expressed in phi units ("size shift"; Garzanti et al., 2008), is readily determined for silt-sized sediments by Stokes' formula and its empirical modifications (Komar and Reimers, 1978). Because turbulence effects cease to be negligible for grains with Reynolds number >0.5 (quartz spheres>80 μm, magnetite spheres>60 μm), size shifts SS_m have to be calculated with empirical formulas for sand. According to Cheng's (1997) formula, tested for natural grains with Corey Shape Factor 0.7, density 2.0–4.3 g/cm^3, and intermediate Reynolds numbers (1<R<1000, corresponding to detrital quartz ~0.1 to ~4 mm in size):

$$SS_m = \mathrm{Log}_2(\Delta_m/\Delta_q) - 3/2\,\mathrm{Log}_2(\Xi_m/\Xi_q), \quad (1)$$

where $\Xi_m = \nu/\eta + ((\nu/\eta)^2 + 48\,(g\cdot\Delta_m/\eta^2)^{2/3})^{1/2}$; ν = settling velocity; g = gravity; Δ_m and Δ_q = submerged densities of mineral m and quartz q (freshwater density = 1 g/cm^3, viscosity η = 0.01 g/cm s).

Eq. (1) does not account for shape differences, and thus provides inaccurate results for mica flakes, settling slower than quartz in spite of their higher density. Size shifts were empirically determined to be −0.2 ± 0.1 ϕ for muscovite, −0.1 ± 0.1 ϕ for biotite, and 0.05 ± 0.1 ϕ for fibrolitic sillimanite in fine to medium sands (Garzanti et al., 2008). Although rough, simple empirical corrections made by assigning fictitious lower densities to non-spherical minerals (e.g., ~2.3 g/cm^3 to muscovite, ~2.5 g/cm^3 to biotite, ~2.8 g/cm^3 to fibrolite) helped reduce discrepancies between theoretical and observed detrital modes of coarser size classes.

Multiple-window analyses of Ganga–Brahmaputra bedload showed excellent size–density correlation for various detrital minerals (r = 0.95 ± 0.02; 0.1% sign. level), and close agreement (−8 ± 7%) between observed and theoretical size-shift coefficients (Fig. 6). Settling equivalence thus explains 91 ± 4% of intrasample mineralogical variability. The small residual discrepancy is largely accounted for by mixing with heavy-mineral-poor finer modes, which decreases size-shift coefficients and goodness of size–density correlations. Size shifts are lower than expected for minerals enriched in the main sand mode, and higher for minerals enriched in finer modes.

Settling-equivalence models for mixtures of two or more subpopulations can be made with a standard spreadsheet if grain size, sorting and mineralogy are known for each subpopulation, and each detrital component is assumed to be lognormally distributed (Garzanti et al., 2009). Observed and predicted mineralogy can thus be compared for each size class of each sample, anomalies due to provenance or shape effects detected, uncertainties in measured textural or mineralogical parameters evaluated, and poorly constrained parameters more accurately determined with best-fit approximations.

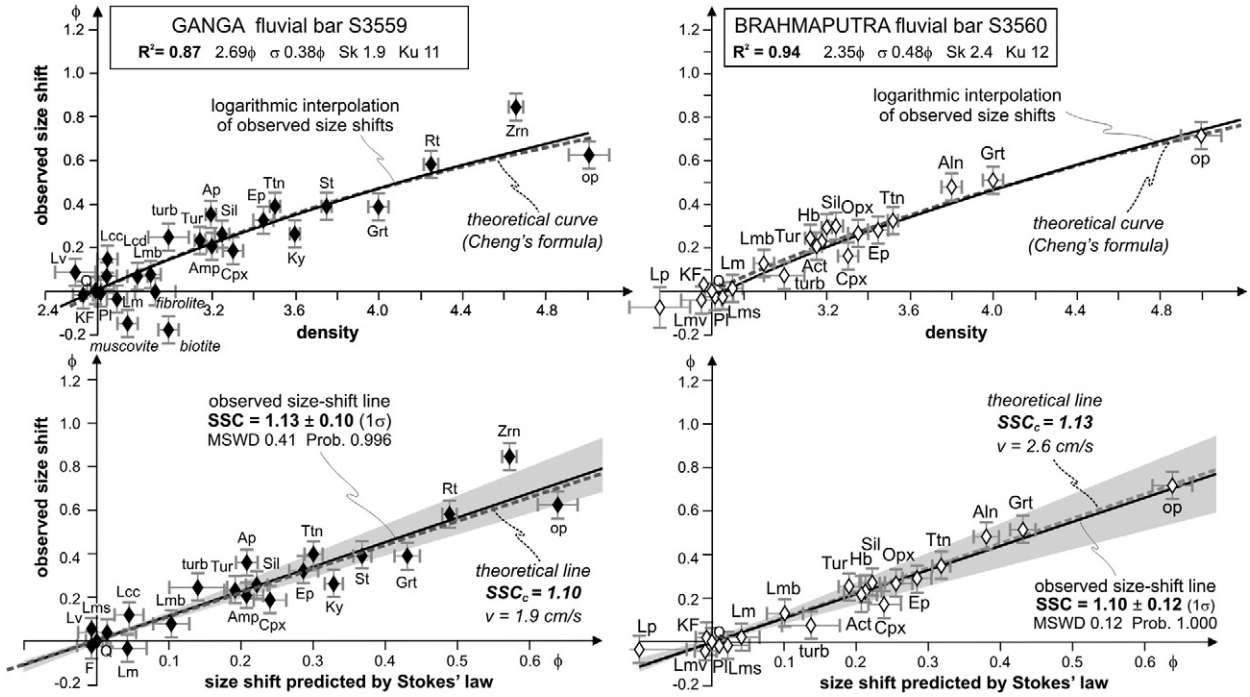

Fig. 6. Settling-equivalence analysis of fluvial-bar deposits. Size–density diagrams (above) and size-shift diagrams (below) indicate that settling equivalence accounts for ~90% of intrasample modal variability. Platy micas and fibrolitic sillimanite were neglected in calculating the coefficient of determination R^2. SSC_c = Size shift coefficient predicted by Cheng's formula; grey areas are 2σ uncertainty envelopes. Size shifts determined by multiple-window analyses at 0.25 ϕ sieve intervals. Textural parameters determined by sieving (σ = sorting value; Sk = skewness; Ku = kurtosis; normal curve has Sk = 0 and Ku = 3). Mineral abbreviations: Act = actinolite; Amp = amphibole; Ap = apatite; Cpx = clinopyroxene; Ep = epidote; F = feldspar; Grt = garnet; Hb = hornblende; KF = K-feldspar; Ky = kyanite; L = lithic grains (Lcc = limestone; Lcd = dolostone; Lmb = metabasite; Lms = low-rank metasedimentary; Lmv = low-rank metavolcanic; Lm = medium- to high-rank metamorphic; Lp = siltstone; Lv = volcanic); op = opaques; Opx = orthopyroxene; Pl = plagioclase; Q = quartz; Rt = rutile; Sil = sillimanite; St = staurolite; Ttn = titanite; Tur = tourmaline; turb = turbid minerals; Zrn = zircon.

Settling-equivalence models for placer BR451, envisaged as a ternary mixture of 93 ± 1% main sand mode with settling velocity 2.1 ± 0.1 cm/s and minor finer modes with settling velocities 1.0 ± 0.2 cm/s and 0.3 ± 0.1 cm/s, predict better size–density correlations than actually observed ($R^2 = 0.9$ vs. 0.7), possibly due to sampling of superposed laminae strictly representing distinct sedimentation units (Otto, 1938). The main sand mode is markedly enriched in heavy minerals (HMC ~ 75) relative to finer modes (HMC ~ 37 and ~10; Fig. 2). Size shifts are high for fibrolite, tourmaline and pyroxene, and low for staurolite, allanite, garnet, rutile, ilmenite and magnetite, indicating stronger concentration of densest minerals in the main sand mode. High size shift for ultradense zircon, ascribed to easier passage through sieve screens of elongated prisms (long axis up to 0.3 mm) and/or limited availability of coarse sizes (Briggs, 1965), is the exception.

5.4. Modeling intrasample chemical variability

The settling-equivalence model can predict chemical composition for each size class of any sample of known mineralogical composition. Uncertainties associated with converting mineralogy into chemistry, however, are superposed on several other approximations (e.g., settling velocities are calculated with empirical formulas; an approximate average density is assigned to each mineral group; shape differences are poorly accounted for; sieves sort grains by shape as well as by size). Even if the occurrence of minor fine modes is neglected for the sake of simplicity, such complexities are difficult to handle also because isomorphous mineral series do not have the same composition in all size classes, denser end-members being concentrated in the fine tail and less dense end-members in the coarse tail. However, assuming for instance different garnet compositions for different classes (i.e., progressively higher almandine component in the fine tail) will add further arbitrariness and only apparent precision, in a process inevitably ending in circular reasoning.

Theoretical and observed chemical compositions of five to nine classes were compared for one fluvial-bar sample from each river and for placer BR451. Even for the extreme intrasample variability displayed by placer deposits, the model successfully reproduces trends of chemical elements hosted in heavy minerals and thus concentrated in the fine tail, hosted in tectosilicates and enriched in the central part of the size distribution, and associated with phyllosilicates and enriched in the coarse tail (Fig. 7). However, the model is sensitive to many imprecisely determined textural, mineralogical, chemical, and physical parameters. Hence, trying to reproduce every detail of the dataset requires a never-ending and ultimately unrewarding effort. We must thus be content with less accurate predictions for intrasample chemical variability than for intrasample mineralogical variability.

6. The mineralogical–chemical budget

A good way to cross-check the robustness and consistency of the several assumptions made is to compare the observed chemical composition of each sample and size class with that recalculated from detrital mineralogy after detrital modes have been converted into weight percentages. This exercise allows us to calibrate percentages of rare detrital minerals such as zircon, titanite, apatite, monazite, xenotime and allanite, which are too rare to be reliably determined with optical analyses but contribute much of key chemical elements (P, Y, REE, Th, U, Zr, Hf) and thus have a significant impact on the chemical budget. REE-bearing minerals carrying radioactive U and Th are widely used in geochronological studies, and precise assessment of their relative abundance in different sources is crucial for the accuracy of provenance diagnoses based on age populations of detrital minerals (Malusà et al., 2009). Moreover, many of them are ultradense, and thus particularly relevant for settling-equivalence analysis. Chemical composition of placer deposits and of their finer size classes allows us to assess how concentration of ultradense minerals varies with varying intensity of hydraulic processes.

6.1. Detrital–mineral contributions

In theory, if mineralogical and chemical composition of each sample and size class are perfectly determined and chemical composition correctly assumed for all detrital components, then we can calculate exactly how much of each element is contributed by each detrital component in each sample and size class. In practice, given the several uncertainties involved, agreement was considered satisfactory for all elements closing on average between 95% and 105% with standard deviation <10% for all samples and size classes. This

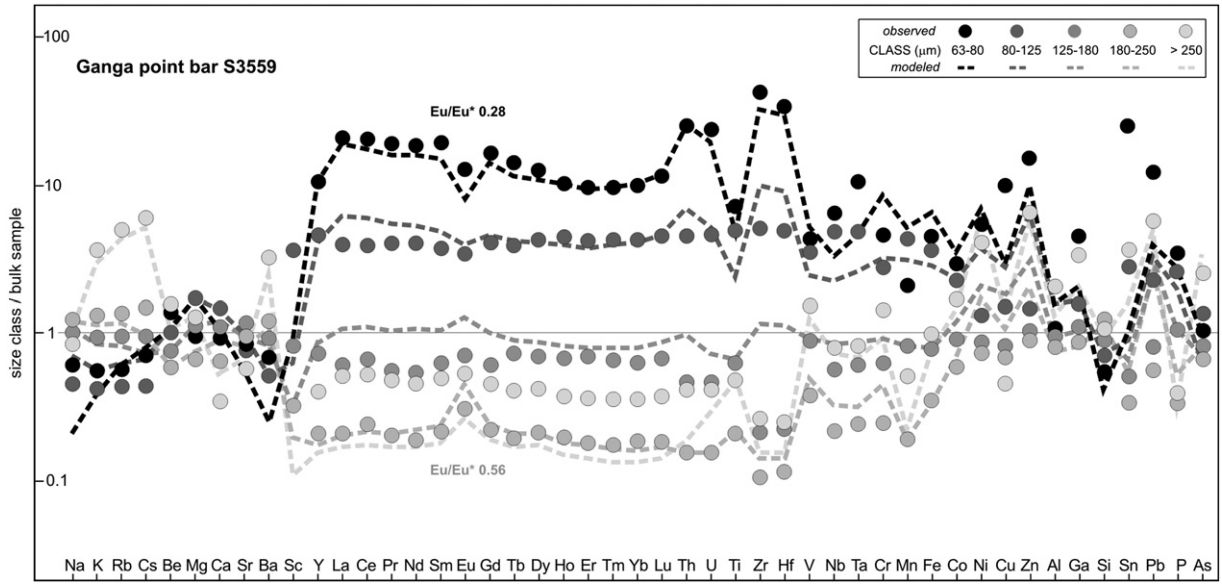

Fig. 7. Modeled versus observed intrasample chemical variability in Ganga bar sample S3559 (elements in multielement diagram normalized to bulk-sample composition). The model reproduces observed trends for most elements. Alkali and alkaline-earth metals, hosted in tectosilicates and phyllosilicates, are enriched in the coarse tail; Y, REE, Th, U, Zr, and Hf, hosted in ultradense zircon, monazite, allanite, and garnet are enriched in the fine tail (but increase again in the mica-dominated coarsest tail). Note hydraulic control on the Eu anomaly, most strongly negative in the finest tail.

could be achieved for most elements, but not for Be, Sc, Mo, W, Cu, Cd, Sn, As, Sb, and Bi, due to insufficiently precise mineralogical or chemical information. Although the same detrital component needs not and does not have the same composition in different rivers (e.g., plagioclase is richer in Ca, Al, Sr in Brahmaputra than in Ganga sands) and different parts of the size distribution (e.g., garnet is richer in Fe and Mn in the fine tail), we assumed the same mineral chemistry for all samples and size classes not to abuse of our liberty of choice. Our best estimates, briefly summarized here below, are given in full in Appendix B.

Quartz contributes most of Si (but ~30% to placer BR451), feldspar most of Na, much of Al, K, Rb, Sr, Ba, and Pb, and significant proportions of Si, Ca, Cs, Eu, and Ga (but minor Si, Al, Ca, Sr, Ga and negligible Eu to placer BR451). Metamorphic and subordinate sedimentary and volcanic lithic grains contribute many elements in significant amounts, micas most of Cs and much of Al, Fe, Mg, K, Ti, Mn, Rb, Ba, V, Nb, Ta, Cr, Mo, W, Co, Ni, Cu, Zn, Cd, Ga, Sn, Pb, and As. Calcite and dolomite contribute much of Ca and Mg to Ganga sand. Amphibole (Fe, Mg, Ca, Ti, Mn, Sc, MREE, V, Cr, Co, Ni, Zn) and epidote contributions (Ca, Sr, Sc, Y, Eu, HREE, V) are higher for Brahmaputra and Padma–Meghna bedload. Garnet contributions (much of Mn and significant Fe, Sc, Y, HREE) are higher for Ganga bedload but reach maximum for Brahmaputra placer BR451. Magnetite contributes significant proportions of Fe, V (much of Fe, V and other transition metals to placer BR451); ilmenite much of Ti, Nb, Ta, Cr (much of Ti, Nb, Ta, and significant Fe, Mg, Mn, V, Cr and other transition metals to placer BR451). Rutile contributes Ti, Nb, Ta. Titanite Ti, MREE, Nb, Ta. Apatite half of P, minor Ca and MREE. Zircon most of Zr, Hf, and significant proportions of Yb, Lu, U, Ta, and Pb (virtually all Zr, Hf to placer BR451). Monazite contributes much of LREE, Th, U (most of LREE, Th, much of MREE, U, P to the finest tail of placer BR451). Allanite also contributes much of LREE, Th. Xenotime much of Y, HREE and significant U. Rare Cr-spinel contributes Cr, tourmaline B, pyroxene minor Mg, Ca, Co, Ni, staurolite minor Zn, kyanite and sillimanite minor Al. Undetected ultradense rare minerals occurring as single grains, inclusions or intergrowths (e.g., cassiterite, wolframite, scheelite, relatively stable sulphides such as sphalerite or arsenopyrite; Craw et al., 2003; Huizing, 1971), may contribute transition metals and other trace elements, as suggested by peak abundances of W, Cd, Sn, Sb, Bi in the finest tail of heavy-mineral-rich samples. Any chemical element is thus contributed by diverse minerals in proportions that change markedly from sample to sample and from size class to size class because of selective-entrainment and settling-equivalence effects, which explains the inadequacy of normative calculations for terrigenous sediments.

7. Selective entrainment and intersample compositional variability

During bedload transport, coarser and less dense detrital minerals are more easily rolled away than smaller and denser grains with which they settled (Slingerland, 1977; Trask and Hand, 1985). Coarser grains are selectively entrained because they project higher above the bed, and hence have smaller pivoting angles and experience greater flow velocities and drag forces (Komar, 2007). Shape is also significant (Winkelmolen, 1982). Rounded spherical particles are rolled more easily than ellipsoidal and angular grains (Hattingh and Illenberger, 1995; Komar and Li, 1986). Size shifts for more spherical minerals are thus expected to be higher in sediments deposited from suspension but lower in sediments modified by traction (Briggs and Middleton, 1965).

Bedload composition and heavy-mineral concentration change continuously in space and time under the whims of turbulent currents. In lag deposits temporarily formed on channel bottoms or bar heads, where velocity increases and erosion prevails, less dense minerals are preferentially removed, and lag deposits enriched in denser minerals to various degrees. In extreme cases, placers are formed (e.g., BR451). Bedload sand hydraulically depleted in heavy minerals also occurs locally (e.g., BR516), as well as phyllosilicate-rich sandy silt or silty sand settled in slack-water conditions and sheltered areas (e.g., BGP5, BR450). Systematic changes in chemical composition correspond to such systematic changes in mineralogical composition.

7.1. Modeling intersample compositional variability

Selective entrainment is difficult to model (Komar, 2007). Nevertheless, modifications of the mineralogical and consequently chemical composition of bedload caused by local changes in current velocity can be readily detected and quantified by calculating the weighted average density of terrigenous grains (SRD index; Garzanti and Andò, 2007):

$$SRD = \sum_{i=1}^{n} (\%m_i \cdot \delta_{mi}), \quad (2)$$

where $\%m$ is the volume percentage of mineral m, and δ_m its density. The SRD index does not correspond exactly to grain density, because intrabasinal and spurious particles (e.g., clay chips, bioclasts, wood fragments, industrial abrasives) are neglected in the calculation.

Because the degree to which any denser mineral lags behind a less dense mineral is a function of their submerged-density ratios (Trask and Hand, 1985), detrital components are systematically enriched in proportion to their density in samples with higher SRD (Garzanti et al., 2009). In order to model compositional variability of bedload, we will first assess the ideal "neutral" SRD and corresponding "neutral" composition that bedload would ideally have everywhere in the absence of selective-entrainment effects. Next, we will calculate predicted changes in mineralogical and chemical composition for increasing concentrations of denser minerals (increasing SRD).

7.2. SRD index of neutral bedload

If a non-porous rock is simply crushed, then the weighted average density of the fragments produced will be equal to the original density of the rock. If downstream fining can be ascribed to pure mechanical grinding, in the absence of hydraulic sorting and chemical weathering, then grain density will remain equal to density of source rocks, as observed in small mountain catchments with cold Alpine climate

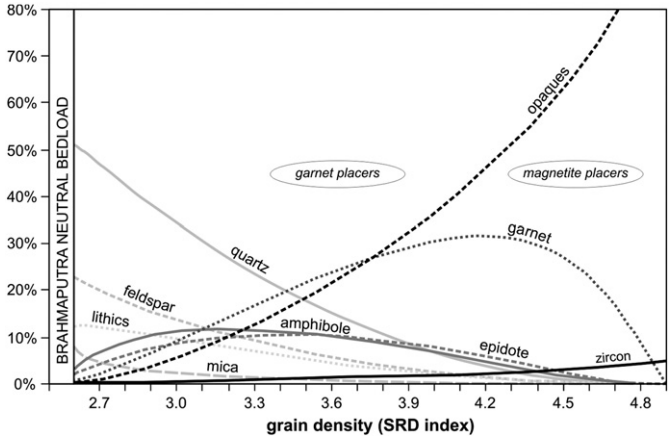

Fig. 8. Predicted mineralogical trends for Brahmaputra bedload. At increasing SRD indices, dense and next ultradense detrital components progressively increase at the expense of mica, quartz, feldspar and lithic grains, to form garnet-rich and finally magnetite-rich placers. Mica decreases at fastest rate to account for easier entrainment of platy grains, as documented by marked phyllosilicate depletion in placer deposits (Garzanti et al., 2009).

(Garzanti et al., 2006). In such conditions, the weighted average density of source rocks can be determined by assessing neutral SRD of detritus, and vice-versa.

In spite of its complex structure, the continental crust displays an overall remarkably regular increase in rock density with tectonostratigraphic depth, anomalies chiefly occurring for cover strata and at local scale (Garzanti et al., 2006). In major river systems draining collision orogens, detritus largely derives from focused erosion of amphibolite-facies gneisses of the axial belt (Galy and France-Lanord, 2001; Garzanti et al., 2007a, 2010). Such mid-crustal rocks contain quartz and feldspar (2.60–2.65 g/cm^3) with 10–15% of denser mica, amphibole, garnet, and epidote; rock density consequently lies in the 2.70–2.75 g/cm^3 range.

Neglecting samples with anomalous heavy-mineral concentration, average SRD of Alpine and Himalayan river bedload is invariably 2.72 ± 0.02 (Garzanti et al., 2004, 2005, 2007b), reflecting modest or mutually compensating influence of detritus from less dense lower-grade rocks exposed in external belts, chemical weathering, and hydraulic processes other than selective entrainment. Fast-settling dense minerals concentrate in bedload, but grain density does not vary much vertically through the water column because suspended load is markedly enriched in slow-settling micas that are also denser than quartz (Garzanti et al., in press). Values in the range 2.72 ± 0.02 can thus be safely assumed as neutral SRD for Ganga–Brahmaputra bedload, also because small differences do not seriously affect calculations.

7.3. Composition of neutral bedload

Elimination of selective-entrainment effects and assessment of neutral-bedload composition allows us to compare sediment petrography, mineralogy and chemistry among different rivers and with crustal standards. Neutral-bedload petrography is calculated by averaging detrital modes of studied samples after neutral SRD is restored for each. This is done by a simple numerical solution, which iteratively corrects abundances of detrital species in proportion to their densities ("SRD correction"; Garzanti et al., 2009). For samples with SRD <neutral SRD:

$$\%m^* = \%m \cdot \delta_m / \sum_{i=1}^{n} (\%m_i \cdot \delta_{mi}), \quad (3)$$

and for samples with SRD>neutral SRD:

$$\%m^* = \%m / \left[\delta_m \cdot \sum_{i=1}^{n} (\%m_i / \delta_{mi})\right]. \quad (4)$$

The SRD correction assumes pure size–density sorting. Diverse behavior of platy, prismatic, spherical, angular or well-rounded minerals may be accounted for empirically by assigning them slightly lower, or slightly higher densities; alternatively, the SRD correction may be applied to detrital modes recalculated on a mica-free basis. Because this procedure is based on several approximations, and successive iterations

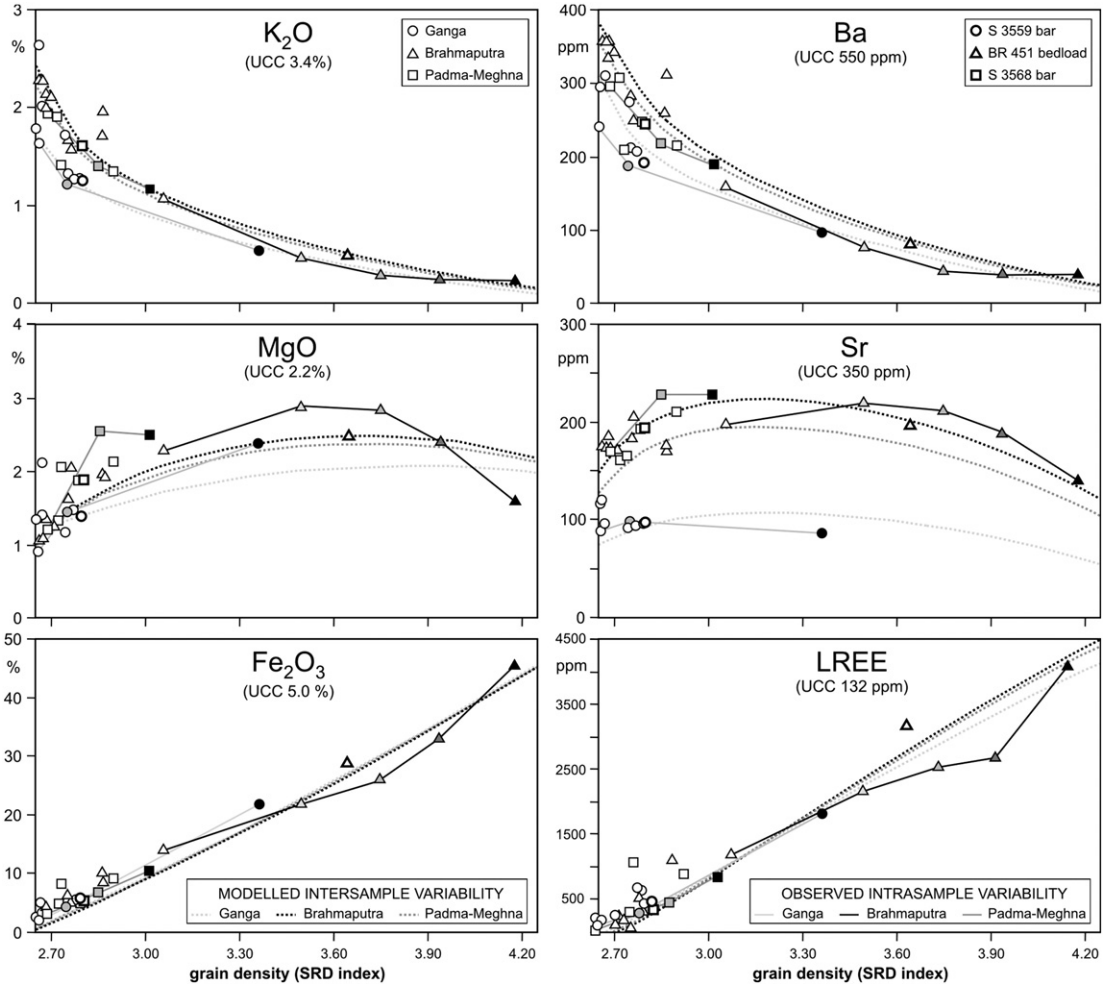

Fig. 9. Predicted versus observed chemical trends for Ganga–Brahmaputra bedload. At increasing SRD indices, elements largely hosted in low-density tectosilicates and platy phyllosilicates decrease exponentially (K, Ba). Elements largely hosted in medium-density minerals such as amphibole and epidote increase to reach maximum in the 3<SRD<4 range and eventually decrease (Mg, Sr). Elements largely hosted in ultradense minerals such as magnetite and monazite increase linearly (Fe, LREE).

amplify errors in initial composition (particularly significant for ill-determined rare minerals), neutral-bedload petrography is assessed roughly. Recalculated chemistry suffers in addition from uncertain assumptions on the chemical composition of detrital components.

An independent alternative way to estimate neutral-bedload composition, needed to test, constrain and refine the results obtained, is offered by information on mineralogy and chemistry of suspended-load, which vary steadily with water depth (Galy et al., 2007). Neutral-bedload composition can be calculated, for instance, by linear regression of mineralogical and chemical data for each vertical profile in each river. Such results are much closer to UCC and much more precise, but not equally accurate, because the relationship between suspended-load composition and water depth becomes markedly non-linear above heavy-mineral-enriched bedload (Garzanti et al., in press). Estimated petrographic, mineralogical and chemical compositions of neutral bedload are given in Appendix C.

7.4. Implications for provenance analysis

Differences in chemical composition between Ganga and Brahmaputra neutral bedload determined with any method remain subtle, indicating effective homogenization of detritus in big river systems draining large continental areas. Systematic differences relative to UCC are limited to depletion in mobile Ca, Na, Sr, and Mo, largely reflecting weathering in tropical monsoonal climates (Kronberg et al., 1987). Si, REE, Zr, and Hf, concentrated in weathering-resistant quartz, monazite, and zircon, are instead moderately enriched. Other elements are hydraulically depleted in bedload because chiefly associated with phyllosilicates preferentially carried in suspension (e.g., Al, Fe, V, Co, Ni, Cu, Zn). Bulk chemistry thus proves to be a blunt tool for provenance analysis, even of non-diagenized sediments. Rather, it represents an exceedingly precious source of information for studying compositional variability associated with weathering and hydraulic sorting.

Effective homogenization of detritus in large river basins implies approximately similar content in accessory minerals such as zircon, apatite or monazite, as confirmed by similar P, REE, Th, U, Zr, and Hf in Ganga and Brahmaputra neutral bedload. This is of consequence for provenance studies based on detrital geochronology. If zircon abundance is similar in Ganga and Brahmaputra sediments, then U/Pb age spectra of Bengal Fan zircons faithfully reflect relative contributions from the two rivers irrespectively of hydraulic effects during turbidite transport and deposition. Instead, in smaller catchments draining crustal sources differently enriched in these elements, and consequently yielding markedly different amounts of REE-bearing minerals (Dickinson, 2008; Moecher and Samson, 2006), provenance analysis is uncertain because hydraulic effects hamper precise assessment of REE-mineral abundances from each catchment (e.g., Amidon et al., 2005).

7.5. Modeling composition of placer deposits

Having determined neutral-bedload mineralogy, we can now theoretically calculate first mineralogical and next chemical composition of sediments progressively enriched in dense and ultradense minerals by stronger and stronger selective-entrainment effects. In successive iterations, detrital minerals are removed at different rates in inverse proportion to their density, and at each step the residual components are recalculated to 100. Shape effects may also be taken into account, flaky particles being lifted more easily and rounded grains rolled away faster than angular grains. At increasing SRD indices, relative abundances of low-density components (e.g., quartz) will decrease exponentially to zero. Conversely, ultradense minerals (e.g., magnetite) will increase exponentially until reaching 100% of the sample (Fig. 8). Components with intermediate density will increase until the density of each is exceeded by the SRD index of the sediment, and eventually will decrease to zero. Enrichment of each single mineral or chemical element predicted for any intensity of selective-entrainment effects can thus be compared with observed compositions in samples with corresponding SRD indices (Fig. 9). In spite of uncertainties in estimating neutral-bedload mineralogy and chemistry of detrital minerals, the model successfully reproduces the observed chemical composition of samples enriched in heavy minerals to various degrees, including placer deposits (Fig. 10).

8. Conclusion

Size–density sorting is by far the major cause of mineralogical and consequently chemical variability in fluvial sediments. Ultradense

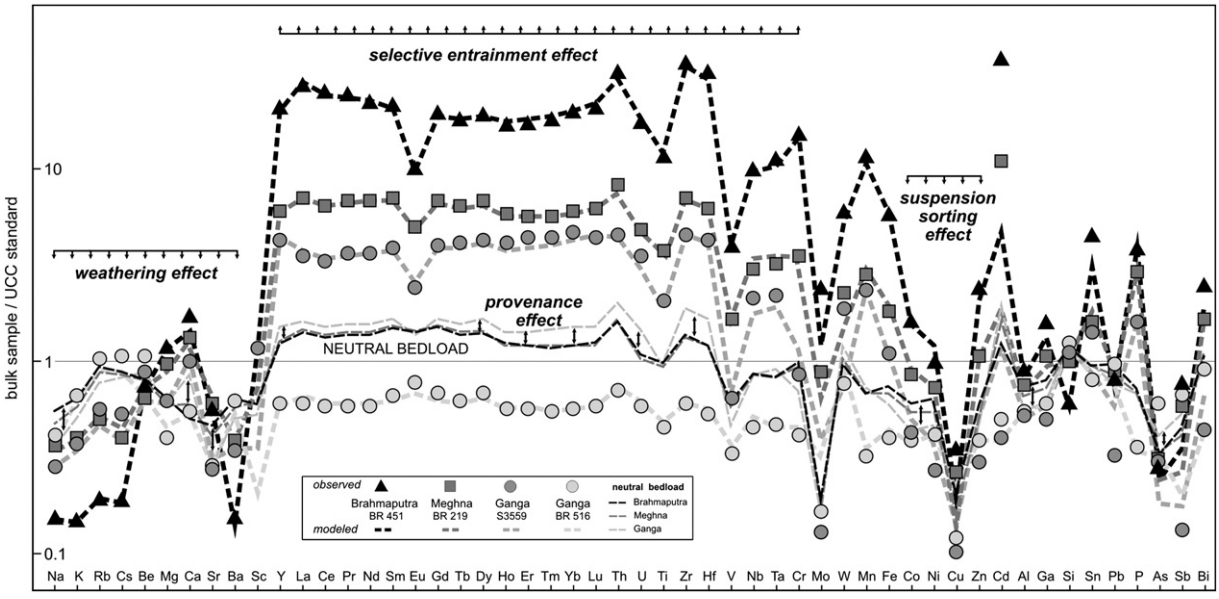

Fig. 10. Modeled versus observed intersample chemical variability of Ganga–Brahmaputra bedload (elements in multielement diagram normalized to UCC). Chemical composition of fluvial sands is chiefly controlled by hydraulic effects superposed on provenance, weathering and anthropic effects. Relative to UCC, neutral bedload is depleted in alkali and alkaline-earth metals because of weathering, and in transition metals associated with clay and oxyhydroxides carried into suspension. Selective-entrainment effects are orders of magnitude greater than subtle provenance-related chemical differences between Ganga and Brahmaputra sands.

minerals such as monazite and zircon, and hence REE, Th, Zr, and Hf, are enriched by more than one order of magnitude in placer lags relatively to neutral bedload and UCC. Enrichment by nearly another order of magnitude occurs in the fine tail of the size distribution. Settling-equivalence and selective-entrainment effects systematically control all chemical parameters, including the Eu anomaly and weathering indices (WIP more than CIA). Hydraulic bias must thus be properly understood and removed before interpreting the mineralogical and chemical composition of sediments to infer geodynamic setting, weathering conditions, or anthropogenic pollution.

By assessing neutral-bedload composition (i.e., mineralogy and chemistry that bedload would have everywhere in the lack of hydraulic effects), weak provenance signals may be depurated from huge hydrodynamic noise, and thus sediment composition compared among diverse rivers or with crustal standards. This can be done both from petrography of bedload samples, reduced to neutral SRD by a simple numerical solution (SRD correction), and from mineralogy and chemistry of suspended-load samples, by calculating the composition at channel-bed depth by linear regression.

Although procedures are empirical and suffer from approximations, modeling compositional variability among samples and size classes represents a useful exercise to test assumptions, assess uncertainties, and ultimately achieve qualitative and quantitative understanding of textural, mineralogical, and chemical changes during transport and deposition. Models reproduce more successfully mineralogical than chemical composition, which suffers from insufficient knowledge of mineral chemistry. By facing the intricacies of the mineralogical–chemical budget, contributions by each detrital mineral can be determined accurately, and abundances of rare REE-bearing minerals commonly used in detrital geochronology calibrated precisely. Compositional variability of sediments is a puzzle with complex design and several pieces lacking, but with patience it can be eventually solved.

Acknowledgments

The article benefited from careful reviews by A. Basu and S.K. Singh. R. Jones (Cairn Energy) and R. Allen kindly provided fluvial-bar samples. Fundamental help was offered by A. Paleari, D. Bersani (Raman analyses), J. Carignan, Y. Harlavan, M. Limonta, M. Padoan, M. Valagussa (chemical analyses), J. Lavé, M. Lupker, M. Campione (physical aspects). CFL and VG were supported by INSU-CNRS program “Reliefs de la Terre”. Prof. M. Rahman (Dhaka University) is warmly thanked for invaluable help in Bangladesh.

Appendix A. Supplementary data

Supplementary data to this article can be found online at doi:10.1016/j.epsl.2010.09.017.

References

Amidon, W.H., Burbank, D.W., Gehrels, G.E., 2005. U–Pb zircon ages as a sediment mixing tracer in the Nepal Himalaya. Earth Planet. Sci. Lett. 235, 244–260.
Andò, S., Bersani, D., Vignola, P., Garzanti, E., 2009. Raman spectroscopy as an effective tool for high-resolution heavy-mineral analysis: examples from major Himalayan and Alpine fluvio-deltaic systems. Spectrochim. Acta A Mol. Biomol. Spectrosc. 73, 450–455.
Ashley, G.M., 1978. Interpretation of polymodal sediments. J. Geol. 86, 411–421.
Bangs Rooney, C., Basu, A., 1994. Provenance analysis of muddy sandstones. J. Sediment. Res. 64, 2–7.
Bea, F., 1996. Residence of REE, Y, Th and U in granites and crustal protoliths; implications for the chemistry of crustal melts. J. Petrol. 35, 521–552.
Best, J.L., Ashworth, P.J., Sarker, M.H., Roden, J.E., 2007. The Brahmaputra–Jamuna River, Bangladesh. In: Gupta, A. (Ed.), Large Rivers: Geomorphology and Management. Wiley, Chichester, pp. 395–433.
Briggs, L.I., 1965. Heavy mineral correlations and provenances. J. Sediment. Petrol. 35, 939–955.
Briggs, L.I., Middleton, G.V., 1965. Hydromechanical principles of sediment structure formation. In: Middleton, G.V. (Ed.), Primary Sedimentary Structures and their Hydrodynamic Interpretations: S.E.P.M. Spec. Publ., 12, pp. 5–16.
Bristow, C.S., 1987. Brahmaputra River; channel migration and deposition. In: Ethridge, F.G., Flores, R.M., Harvey, M.D., Weaver, J.N. (Eds.), Recent Developments in Fluvial Sedimentology: Soc. Econ. Paleont. Miner. Spec. Publ., 39, pp. 63–74.
Carignan, J., Hild, P., Mevelle, G., Morel, J., Yeghicheyan, D., 2001. Routine analyses of trace element in geological samples using flow injection and low pressure on-line liquid chromatography coupled to ICP-MS: a study of geochemical reference materials BR, DR-N, UB-N, AN-G and GH. Geostandard. Newslett. 25, 187–198.
Cheng, N.-S., 1997. Simplified settling velocity formula for sediment particle. J. Hydraul. Eng. 123, 149–152.
Cohen, D., Ward, C.R., 1991. SEDNORM—a program to calculate a normative mineralogy for sedimentary rocks based on chemical analysis. Comput. Geosci. 17, 1235–1253.
Coleman, J.M., 1969. Brahmaputra River: channel processes and sedimentation. Sediment. Geol. 3, 129–239.
Condie, K.C., 1993. Chemical composition and evolution of the upper continental crust: contrasting results from surface samples and shales. Chem. Geol. 104, 1–37.
Cox, R., Lowe, D.R., 1996. Quantification of the effects of secondary matrix on the analysis of sandstone composition, and a petrographic-chemical technique for retrieving original framework grain modes of altered sandstone. J. Sediment. Res. 66, 548–558.
Craw, D., Falconer, D., Youngson, J.H., 2003. Environmental arsenopyrite stability and dissolution: theory, experiment, and field observations. Chem. Geol. 199, 71–82.
Cullers, R.L., 1995. The controls on the major- and trace-element evolution of shales, siltstones and sandstones of Ordovician to Tertiary age in the Wet Mountains region, Colorado, U.S.A. Chem. Geol. 123, 107–131.
Dickinson, W.R., 1970. Interpreting detrital modes of graywacke and arkose. J. Sediment. Res. 40, 695–707.
Dickinson, W.R., 2008. Impact of differential zircon fertility of granitoid basement rocks in North America on age populations of detrital zircons and implications for granite petrogenesis. Earth Planet. Sci. Lett. 275, 80–92.
Fedo, C.M., Nesbitt, H.W., Young, G.M., 1995. Unraveling the effects of potassium metasomatism in sedimentary rocks and paleosols, with implications for paleo-weathering conditions and provenance. Geology 23, 921–924.
France-Lanord, C., Derry, L.A., 1997. Organic carbon burial forcing of the carbon cycle from Himalayan erosion. Nature 390, 65–67.
France-Lanord, C., Derry, L., Michard, A., 1993. Evolution of the Himalaya since Miocene time: isotopic and sedimentological evidence from the Bengal Fan. In: Treloar, P.J., Searle, M.P. (Eds.), Himalayan Tectonics: Geol. Soc. London Spec. Publ., 74, pp. 603–622.
Friedman, G.M., 1967. Dynamic processes and statistical parameters compared for size frequency distributions of beach and river sands. J. Sediment. Petrol. 37, 327–354.
Galy, A., France-Lanord, C., 1999. Weathering processes in the Ganges–Brahmaputra basin and the riverine alkalinity budget. Chem. Geol. 159, 31–60.
Galy, A., France-Lanord, C., 2001. Higher Erosion rates in the Himalaya: geochemical constraints on riverine fluxes. Geology 29, 23–26.
Galy, A., France-Lanord, C., Derry, L.A., 1999. The strontium isotopic budget of Himalayan Rivers in Nepal and Bangladesh. Geochim. Cosmochim. Acta 63, 1905–1925.
Galy, V., France-Lanord, C., Beyssac, O., Faure, P., Kudrass, H., Palhol, F., 2007. Efficient organic carbon burial in the Bengal fan sustained by the Himalayan erosional system. Nature 450, 407–410.
Gansser, A., 1964. Geology of the Himalayas. Wiley, New York. 289 pp.
Garzanti, E., Andò, S., 2007. Heavy-mineral concentration in modern sands: implications for provenance interpretation. In: Mange, M.A., Wright, D.T. (Eds.), Heavy Minerals in Use. : Developments in Sedimentology Series, 58. Elsevier, Amsterdam, pp. 517–545.
Garzanti, E., Vezzoli, G., Andò, S., France-Lanord, C., Singh, S.K., Foster, G., 2004. Sand petrology and focused erosion in collision orogens: the Brahmaputra case. Earth Planet. Sci. Lett. 220, 157–174.
Garzanti, E., Vezzoli, G., Andò, S., Paparella, P., Clift, P.D., 2005. Petrology of Indus River sands: a key to interpret erosion history of the Western Himalayan Syntaxis. Earth Planet. Sci. Lett. 229, 287–302.
Garzanti, E., Andò, S., Vezzoli, G., 2006. The continental crust as a source of sand (Southern Alps cross-section, Northern Italy). J. Geol. 114, 533–554.
Garzanti, E., Doglioni, C., Vezzoli, G., Andò, S., 2007a. Orogenic belts and orogenic sediment provenances. J. Geol. 115, 315–334.
Garzanti, E., Vezzoli, G., Andò, S., Lavé, J., Attal, M., France-Lanord, C., DeCelles, P., 2007b. Quantifying Sand Provenance and Erosion (Marsyandi River, Nepal Himalaya). Earth Planet. Sci. Lett. 258, 500–515.
Garzanti, E., Andò, S., Vezzoli, G., 2008. Settling-equivalence of detrital minerals and grain-size dependence of sediment composition. Earth Planet. Sci. Lett. 273, 138–151.
Garzanti, E., Ando', S., Vezzoli, G., 2009. Grain-size dependence of sediment composition and environmental bias in provenance studies. Earth Planet. Sci. Lett. 277, 422–432.
Garzanti, E., Resentini, A., Vezzoli, G., Andò, S., Malusà, M.G., Padoan, M., Paparella, P., 2010. Detrital fingerprints of fossil continental-subduction zones (Axial Belt Provenance, European Alps). J. Geol. 118, 341–362.
Garzanti, E., Andò, S., France-Lanord, C., Galy, V., Censi, P., Vignola, P., in press. Mineralogical and chemical variability of fluvial sediments. 2. Suspended-load silt (Ganga-Brahmaputra, Bangladesh). Earth Planet. Sci. Lett.
Goodbred, S.L., Kuehl, S.A., 2000. Enormous Ganges-Brahmaputra sediment discharge during strengthened early Holocene monsoon. Geology 28, 1083–1086.
Govindaraju, K., Mevelle, G., 1987. Fully automated dissolution and separation methods for inductively coupled plasma-atomic emission spectrometry rock analysis.

Application to the determination of rare earth elements. J. Anal. Atom. Spectrom. 2, 615–621.
Hattingh, J., Illenberger, W.K., 1995. Shape sorting of flood-transported synthetic clasts in a gravel bed river. Sediment. Geol. 96, 181–190.
Hay, W.W., 1998. Detrital sediment fluxes from continents to oceans. Chem. Geol. 145, 287–323.
Hering, O.H., Zimmerle, W., 1963. Simple method of distinguishing zircon, monazite, and xenotime. J. Sediment. Res. 33, 472–473.
Heroy, D.C., Kuehl, S.A., Goodbred, S.L., 2003. Mineralogy of the Ganges and Brahmaputra Rivers: implications for river switching and Late Quaternary climate change. Sediment. Geol. 155, 343–359.
Hu, Z., Gao, S., 2008. Upper crustal abundances of trace elements: a revision and update. Chem. Geol. 253, 205–221.
Huizing, H.G.J., 1971. A reconnaissance study of the mineralogy of sand fractions from East Pakistan sediments and soils. Geoderma 6, 109–133.
Ingersoll, R.V., Bullard, T.F., Ford, R.L., Grimm, J.P., Pickle, J.D., Sares, S.W., 1984. The effect of grain size on detrital modes: a test of the Gazzi-Dickinson point-counting method. J. Sediment. Petrol. 54, 103–116.
Ingersoll, R.V., Dickinson, W.R., Graham, S.A., 2003. Remnant-ocean submarine fans: largest sedimentary systems on Earth. In: Chan, M.A., Archer, A.W. (Eds.), Extreme Depositional Environments: Mega End Members in Geologic Time: Geol. Soc. Am. Spec. Pap., 370, pp. 191–208.
Islam, M.R., Begum, S.F., Yamaguchi, Y., Ogawa, K., 1999. The Ganges and Brahmaputra rivers in Bangladesh: basin denudation and sedimentation. Hydrol. Process. 13, 2907–2923.
Komar, P.D., 2007. The entrainment, transport and sorting of heavy minerals by waves and currents. In: Mange, M.A., Wright, D.T. (Eds.), Heavy Minerals in Use. Developments in Sedimentology Series, 58. Elsevier, Amsterdam, pp. 3–48.
Komar, P.D., Li, Z., 1986. Pivoting analyses of the selective entrainment of sediments by shape and size with application to gravel threshold. Sedimentology 33, 425–436.
Komar, P.D., Reimers, C.E., 1978. Grain shape effects on settling rates. J. Geol. 86, 193–209.
Kronberg, B.I., Nesbitt, H.W., Fyfe, W.S., 1987. Mobilities of alkalis, alkaline earths and halogens during weathering. Chem. Geol. 60, 41–49.
Malusà, M.G., Zattin, M., Andò, S., Garzanti, E., Vezzoli, G., 2009. Focused erosion in the Alps constrained by fission-track ages on detrital apatites. In: Lisker, F., Ventura, B., Glasmacher, U.A. (Eds.), Thermochronological Methods: From Palaeotemperature Constraints to Landscape Evolution Models: Geol. Soc. London Spec. Publ., 324, pp. 141–152.
Mange, A., Maurer, H.F.W., 1992. Heavy Minerals in Colour. Chapman and Hall, London. 147 pp.
Matlack, K.S., Houseknecht, D.W., Applin, K.R., 1989. Emplacement of clay into sand by infiltration. J. Sediment. Petrol. 59, 77–87.
McDonough, W.F., Sun, S.S., 1995. The composition of the Earth. Chem. Geol. 120, 223–253.
McLennan, S.M., 1989. Rare earth elements in sedimentary rocks: influence of provenance and sedimentary processes. Rev. Mineral. Geochem. 21, 169–200.
McLennan, S.M., 2001. Relationships between the trace element composition of sedimentary rocks and upper continental crustr. Geochem. Geophys. Geosyst. 2 2000GC000109.
McLennan, S.M., Hemming, S., McDaniel, D.K., Hanson, G.N., 1993. Geochemical approaches to sedimentation, provenance and tectonics. In: Johnsson, M.J., Basu, A. (Eds.), Processes Controlling the Composition of Clastic Sediments: Geol. Soc. Am. Spec. Pap., 284, pp. 21–40.
Middleton, G.V., 1976. Hydraulic interpretation of sand size distributions. J. Geol. 84, 405–426.
Moecher, D.P., Samson, S.D., 2006. Differential zircon fertility of source terranes and natural bias in the detrital zircon record: implications for sedimentary provenance analysis. Earth Planet. Sci. Lett. 247, 252–266.
Mongelli, G., Critelli, S., Perri, F., Sonnino, M., Perrone, V., 2006. Sedimentary recycling, provenance and paleoweathering from chemistry and mineralogy of Mesozoic continental redbed mudrocks, Peloritani mountains, southern Italy. Geochem. J. 40, 197–209.
Nesbitt, H.W., Young, G.M., 1982. Early Proterozoic climates and plate motions inferred from major element chemistry of lutites. Nature 299, 715–717.
Ohta, T., 2004. Geochemistry of Jurassic to earliest Cretaceous deposits in the Nagato Basin, SW Japan: implication of factor analysis to sorting effects and provenance signatures. Sediment. Geol. 171, 159–180.
Otto, G.H., 1938. The sedimentation unit and its use in field sampling. J. Geol. 46, 569–582.
Paktunc, A.D., 2001. MODAN — a computer program for estimating mineral quantities based on bulk composition: windows version. Comput. Geosci. 27, 883–886.
Parker, A., 1970. An index of weathering for silicate rocks. Geol. Mag. 107, 501–504.
Price, J.R., Velbel, M.A., 2003. Chemical weathering indices applied to weathering profiles developed on heterogeneous felsic metamorphic parent rocks. Chem. Geol. 202, 397–416.
Rittenhouse, G., 1943. Transportation and deposition of heavy minerals. Geol. Soc. Am. Bull. 54, 1725–1780.
Rosen, O.M., Abbyasov, A.A., Tipper, J.C., 2004. MINLITH—an experience-based algorithm for estimating the likely mineralogical compositions of sedimentary rocks from bulk chemical analyses. Comput. Geosci. 30, 647–661.
RSP (River Survey Project), 1996. Spatial representation and analysis of hydraulic and morphological data. Report n° FAP 24. WARPO, Dhaka, Bangladesh.
Rubatto, D., 2002. Zircon trace element geochemistry: partitioning with garnet and the link between U–Pb ages and metamorphism. Chem. Geol. 184, 123–138.
Rubey, W.W., 1933. The size-distribution of heavy minerals within a water-laid sandstone. J. Sediment. Petrol. 3, 3–29.
Schuiling, R.D., de Meijer, R.J., Riezebos, H.J., Scholten, M.J., 1985. Grain size distribution of different minerals in a sediment as a function of their specific density. Geol. Mijnbow 64, 199–203.
Singh, I.B., 2007. The Ganga River. In: Gupta, A. (Ed.), Large rivers: geomorphology and management. Wiley, Chichester, pp. 347–371.
Singh, P., 2009. Major, trace and REE geochemistry of the Ganga River sediments: influence of provenance and sedimentary processes. Chem. Geol. 266, 251–264.
Singh, S.K., France-Lanord, C., 2002. Tracing the distribution of erosion in the Brahmaputra watershed from isotopic compositions of stream sediments. Earth Planet. Sci. Lett. 202, 645–662.
Singh, S.K., Sarin, M.M., France-Lanord, C., 2005. Chemical erosion in the eastern Himalaya: major ion composition of the Brahmaputra and $\delta^{13}C$ of dissolved inorganic carbon. Geochim. Cosmochim. Acta 69, 3573–3588.
Singh, S.K., Rai, S.K., Krishnaswami, S., 2008. Sr and Nd isotopes in river sediments from the Ganga basin: sediment provenance and spatial variability in physical erosion. J. Geophys. Res. 113, F03006. doi:10.1029/2007/JF000909.
Slaughter, M., 1989. Quantitative determination of clays and other minerals in rocks. Clay Min. Soc. Workshop Lect. 1, 120–151.
Slingerland, R., 1977. The effects of entrainment on the hydraulic equivalence relationships of light and heavy minerals in sands. J. Sediment. Petrol. 47, 753–770.
Spencer, D.W., 1963. The interpretation of grain size distribution of curves of clastic sediments. J. Sediment. Petrol. 33, 180–190.
Sun, D., Bloemendal, J., Rea, D.K., Vandenberghe, J., Jiang, F., An, Z., Su, R., 2002. Grain-size distribution function of polymodal sediments in hydraulic and aeolian environments, and numerical partitioning of the sedimentary components. Sediment. Geol. 152, 263–277.
Tanner, W.F., 1964. Modification of sediment size distributions. J. Sediment. Petrol. 34, 156–164.
Taylor, S.R., McLennan, S.M., 1995. The geochemical evolution of the continental crust. Rev. Geophys. 33, 241–265.
Trask, C.B., Hand, B.M., 1985. Differential transport of fall-equivalent sand grains, Lake Ontario, New York. J. Sediment. Petrol. 55, 226–234.
Vanoni, V.A., 2006. Sedimentation engineering. ASCE Manuals and Reports in Engineering Practice, 54. Am. Soc. Civ. Eng, Reston. 418 pp.
Winkelmolen, A.M., 1982. Critical remarks on grain parameters, with special emphasis on shape. Sedimentology 29, 255–265.